Eur. Phys. J. C 45, 61–72 (2006)
Digital Object Identifier (DOI) 10.1140/epjc/s2005-02414-7

THE EUROPEAN
PHYSICAL JOURNAL C

Soft hadron ratios at the LHC

J. Rafelski[1,a], J. Letessier[2]

[1] Department of Physics, University of Arizona, Tucson, Arizona, 85721, USA
[2] Laboratoire de Physique Théorique et Hautes Energies, Université Paris 7, 2 place Jussieu, 75251 Cedex 05, France

Received: 17 June 2005 / Revised version: 29 September 2005 /

Abstract. High precision soft hadron abundance data produced in relativistic nuclear collisions at LHC at $\sqrt{s_{\rm NN}} \le 5500\,$GeV will become available beginning in 2007/8. We explore, within the statistical hadronization model, how these results can help us understand the properties of the deconfined quark–gluon phase at its breakup. We make assumptions about the physical properties of the fireball and obtain particle production predictions. Then, we develop a strategy to measure parameters of interest, such as strangeness occupancy γ_s, chemical potentials $\mu_{\rm B}$ and μ_S.

PACS. 24.10.Pa, 25.75.-q

1 Introductory remarks

The relativistic heavy-ion collisions experimental program has as its objective the formation of the deconfined quark–gluon plasma (QGP) phase in the laboratory. The uncertainty in this experimental program is if, in the available short collision time, 10^{-22}–10^{-23} s, the color frozen nuclear phase can melt and turn into the QGP state of matter. There is no valid first principle answer available today, nor it seems, can it be expected in the foreseeable future. From this, and other such uncertainties about the QGP, arises the need to define and study its observables, even though we are quite convinced that this is the state of matter that filled the Universe in its early stage, till hadronization occurred 10–20 μs into its evolution. QGP is the *equilibrium* state in a hot Universe at temperature above that of the lightest hadronic particle, the pion, $kT > m_\pi c^2 = 140\,$MeV (we from now on use units such that $k = c = \hbar = 1$).

A detailed theoretical study of the properties of this new state of matter shows that QGP is rich in entropy and strangeness. These are the observables discussed here explicitly, and implicitly, in the context of soft hadron production. The enhancement of the entropy S arises in the early stages of the collision process, because the color bonds are broken, and numerous gluons are formed and thermalized. Enhancement of the strangeness s is in part also due to the breaking of the color bonds. Furthermore, it is due to a modification of the kinetic strangeness formation processes. These operate faster in the deconfined phase, mainly because the mass threshold for strangeness excitation is considerably lower in QGP than in hadron matter, but also because there are more channels available considering the color quantum numbers.

We will not discuss the following important QGP observables in this work, their current status at RHIC is discussed, e.g., in [1]. Aside from strangeness and entropy enhancement, another soft hadron signature is the shape of the particle spectra, which carries information about the formation and evolution dynamics of the state of matter that is the source of these particles. Given the considerable increased energy, we expect a greater energy density in the initial stage, and thus a much more violent transverse outflow of matter than has been seen at RHIC. Such a strange transverse collective flow carries many particles to high transverse momenta and produces a strong azimuthal asymmetry in particle spectra for finite impact parameter reactions. Among other related hadronic signatures, we note a significant charm quark abundance, originating in primary parton reactions. The pattern of charm hadronization should reveal further details about the QGP phase, just as strange hadrons do.

Within a few years, a new energy domain will become accessible in the study of heavy-ion collisions, when the Large Hadron Collider (LHC) at CERN becomes operational in 2007. The top energy available to Pb–Pb reactions is $\sqrt{s_{NN}} = 5500\,$GeV, a 27.5-fold increase compared to the top RHIC energy. Extrapolating the trends of SPS and RHIC physics, we expect much greater entropy and strangeness yields at central rapidity. We will always address, in this work, most central head on collision reactions of two $A \simeq 200$ heavy nuclei; at LHC this will be a Pb–Pb collision .

At these high energies, there will be much less stopping power of baryon number, and thus the central rapidity region will be much more similar to the phase prevailing in the early Universe than this is the case at RHIC. One of the objectives of this work is to assess how small the baryochemical potential $\mu_{\rm B}$ can become, compared to

---

[a] e-mail: Johann.Rafelski@cern.ch

$\mu_{\rm B} \simeq 25\,\mathrm{MeV}$ observed at RHIC. The scale of $\mu_{\rm B}$ at the hadronization of the early Universe is $\mu_{\rm B}^{\rm U} \simeq 1\,\mathrm{eV}$ [2].

In this paper, we address specifically the pattern of soft hadron production based on the assumption of a sudden breakup of the deconfined hadron phase with all soft hadrons produced at essentially the same physical conditions, and not subject to the requirement of the absolute chemical equilibrium condition. We will, however, provide reference data for the chemical equilibrium case. In Sect. 2, we outline the statistical hadronization model and present its parameters. In Sect. 3, we discuss how simple, but general, hypotheses allow one to fix values of these parameters. We establish the range of physical interest for the strangeness phase space occupancy γ_s. In Sect. 4, we develop our predictions regarding the properties of the hadronizing fireball. We present the range of statistical parameters which we expect and the physical properties of the fireball at its breakup. We consider particle ratios which could help determine the value of γ_s, which is a parameter in this study. In Sect. 5, we consider the observables sensitive to $\mu_{\rm B}$ and obtain results which show how precise the hadron yields need to be measured in order to allow for measurement of $\mu_{\rm B}$.

2 Statistical hadronization and model parameters

The statistical hadronization model (SHM) is, by definition, a model of particle production in which the formation process of each particle fully saturates (maximizes) the quantum mechanical probability amplitude. Particle yields are thus determined by the appropriate integrals of the accessible phase space [3]. For a system subject to global dynamical evolution, such as collective flow, this applies within each volume element, in its local rest frame of reference. The SHM is consistent with the wealth of SPS and RHIC data available today. A systematic study of the particle production for a wide reaction energy range confirms the applicability of the SHM [4, 5].

Analysis of hadron yields further facilitates a study of the physical properties of the hadronic fireball at the time of hadronization, when these particles are produced, i.e., undergo chemical freeze-out. A study of hadron multiplicities, produced at energy ranging from the top of AGS energy to the top of RHIC energy, leads to an understanding of the physical properties of the fireball at hadronization [4]. Here, we reverse the approach – using the systematics of the energy dependence of the physical properties of the fireball, we establish our expectations about the statistical parameters and relative particle multiplicities expected at LHC. We cannot address, in this work, the total hadron yield, since this depends on the early stage of the reaction, and specifically, on the entropy formation process in the initial interactions.

The complexity of the SHM model derives from the need to account for many hadronic resonances and their decays. Since the number of massive resonances grows exponentially, their contributions to particle yields, especially to the yields of pions, are slowly convergent. Moreover, the counting of resonances and their conserved quantum numbers poses a significant book keeping challenge. For this reason, an effort has been made to generate a comprehensive software package available to all interested parties, with a transparent hadron data input, and a comprehensive parameter field. All results presented were obtained using this numerical package SHARE (statistical hadronization with resonances) [6].

A package of similar capability, but with restrained parameter set, has since become available [7]. These programs are including a large number of resonances and track the chemical composition as well as the decay trees with care. As a result, the benchmark fits produce a hadronization temperature which is considerably lower than obtained in [5] for the SPS or RHIC reaction systems.

A successful description of rapidity particle yields within the SHM, at a single-chemical freeze-out condition, produces the model parameters in the process of χ^2 minimization. The parameters are

(1) $\mathrm{d}V/\mathrm{d}y$, the volume related a given rapidity to the particle yields;

(2) T, the (chemical) freeze-out temperature;

(3) $\mu_{\rm B} \equiv T \ln(\lambda_u \lambda_d)^{3/2}$, the baryon and

(4) $\mu_S \equiv T \ln[\lambda_q/\lambda_s]$, the hyperon chemical potentials;

(5) $\lambda_{I3} \equiv \lambda_u/\lambda_d$, a fugacity distinguishing the up from the down quark flavor;

(6) γ_s, the strangeness phase space occupancy;

(7) γ_q, the light quark phase space occupancy.

When the assumption of absolute chemical equilibrium is made, the values $\gamma_s = \gamma_q = 1$ are set. The relationship to the quark flavor fugacities $\lambda_i, i = u, d, s$ is made explicit above.

When a set of parameters is known, all particle multiplicities can be evaluated exactly. Similarly, one can obtain the physical properties of the fireball such as thermal energy, entropy and baryon content by an appropriate evaluation of the properties of the partial fraction contributions of each hadronic state. In that way, in fact, one obtains from a fit to a limited set of measured particle yields a full phase space extrapolation for any particle yield, and a full understanding of the properties of the fireball. Some striking "conservation of fireball properties" rules emerged from such an analysis of particle yield data [4], and these we will use in order to predict the (relative) particle yields at the LHC energy range.

3 LHC hadronization

3.1 Choice of conditions and constraints

To predict the seven parameters, at first sight, we need at least seven, and better more than that, valid conditions, constraints and hypotheses.

(1) The "volume" normalization $\mathrm{d}V/\mathrm{d}y$ only enters absolute hadron yields. Consequently, it is related to the initial conditions, i.e., mechanisms of entropy production. Restricting our investigation to the study of particle ratios,

we do not need to know the value of this parameter, which normalizes the overall yield.

Next, there are two natural physics constraints.

(2) Strangeness conservation, i.e., the (grand canonical) count of s quarks in hadrons equals the $\bar{s}$ count at each rapidity unit. In our specific case, we request that

$$\frac{\bar{s}-s}{\bar{s}+s} = 0 \pm 0.01. \qquad (1)$$

We will show in some detail in Sect. 5.1 how this condition establishes the relationship between the baryochemical potential μ_{B} and the strangeness chemical potential μ_S.

(3) The electrical charge-to-net baryon ratio, in the final state, should be the same as in the initial state, and in the specific case of Pb–Pb interactions, we have

$$\frac{Q}{b} = 0.39 \pm 0.01. \qquad (2)$$

The 2.5% error can be seen as expressing the uncertainty about how well neutron and proton densities follow each other, given that even most central reactions occur at finite impact parameter, and 10% of the nucleons do not participate in the reaction.

(4) and (5)

(i) The phase space occupancy parameters in some approaches are tacitly fixed: assuming the chemical equilibrium one sets

$$\gamma_s = \gamma_q = 1.$$

(ii) In the chemical non-equilibrium approach, the systematics of data analysis at RHIC and high SPS energies firmly predicts

$$\gamma_q \simeq \mathrm{e}^{m_{\pi^0}/2T}.$$

Furthermore, we will present our results as a function of γ_s. We believe that the value of γ_s is linked to the collision energy, as more strangeness can be produced when the initial conditions reached become more extreme. We show, in Sect. 4.2, how γ_s fixes several easily accessible observables and can be measured, and the consistency of the chemical non-equilibrium approach checked. At LHC energy, the expected value of γ_s is so much greater than unity, and thus, we can be sure that a distinction from $\gamma_s = 1$ for the equilibrium model can be arrived at in an unambiguous way.

There are (at least) two further conditions required which must be sensitive to the hadronization temperature and baryochemical potential. These will be drawn from the following observations.

(6) We note the value,

$$\frac{E}{TS} \to 0.78, \quad \text{or} \to 0.845,$$

for chemical non-equilibrium [4], or respectively, equilibrium model analysis. We note that the energy per particle of non-relativistic and semi-relativistic classical particle gas is $E/N \simeq m + 3/2\,T + \ldots$, while the entropy per particle in this condition is $S/N = 5/2 + m/T + \ldots$ (see Sect. 10 of [3]). Hence we have

$$\frac{E}{TS} \simeq \frac{m/T + 3/2}{m/T + 5/2}. \qquad (3)$$

It is thus possible to interpret this constraint in terms of the quark matter made of particles with thermal mass $m \propto aT$. Solving (3), we find for $E/TS = 0.78$ $a = 2$ for chemical non-equilibrium, and for $E/TS = 0.845$ $a = 4$ for equilibrium. This is close to the result expected in finite temperature QCD [8]. That result points to a simple structure of the quark matter fireball. On the quark-side, the value E/TS is not very model specific, though it is sensitive to the average particle mass as shown above.

On the other hand, there is considerable sensitivity to this thermodynamic constraint in the hadronic gas. The hadron system after hadronization comprises a mix of particles of different, and for the baryon component, large mass. To fine-tune this value a specific ratio of baryons to mesons needs to be established: in this way the hadron system can maintain both energy and entropy, aside of baryon number and strangeness, during hadronization. For this reason, in the hadron phase there is considerable sensitivity of this ratio to both T and the value of the phase space occupancy parameters, here γ_s.

(7) We need to make an assumption which fixes the baryochemical potential μ_{B}. This certainly is one of most difficult guesses as there is no reliable way to predict baryon stopping at LHC, and certainly this value,

$$\mu_{\mathrm{B}} \ll T,$$

will be quite difficult to measure. For this reason, we will discuss, in Sect. 5, at length a method to measure μ_{B}. The impact of $\mu_{\mathrm{B}} \simeq 1$–$3\,\mathrm{MeV}$ on mixed particle ratios, such as K/π or η/π^0 is physically irrelevant. We will show how particle–antiparticle abundances can help us further. In fact, it is uncertain that a measurement of such a small μ_{B} can be accomplished, and thus in effect, we could have simply assumed $\mu_{\mathrm{B}} = 0$ which at a few %-level would be consistent with all relative hadron yield predictions here presented. On the other hand, the understanding of the matter–antimatter asymmetry present at the LHC energy scale is, in itself, of interest and thus, we pursue this question further.

We argue as follows: our analysis of RHIC data suggested that baryons are more easily retained in the central rapidity region than energy, with a 2.5 times larger fraction of colliding baryons than the fraction of energy deposited. Considering the SPS data point, and the RHIC results, the per baryon thermalized reaction energy retained in the central rapidity region, in units of the maximum available collision energy, drops from 40% available at RHIC to 15% at LHC. Given the LHC energy $\sqrt{s_{NN}} = 5500\,\mathrm{GeV}$, a thermal energy content per net baryon at $y = 0$ is assumed to be

$$\frac{\mathrm{d}E}{\mathrm{d}b} = 0.15 \times 5500/2 = 412 \pm 20\,\mathrm{GeV},$$

at top LHC energy, where the error is chosen to be similar in relative magnitude as the error in other observables considered. This error plays a role in finding the solution in terms of statistical variables of the constraints and conditions considered.

This specific assumption fixes implicitly the (small) value of the baryochemical potential, and by virtue of the strangeness conservation, also of the strange chemical potential. When we deviate from this assumption in exploring a wider parameter range, we will mention this explicitly.

3.2 η and maximum value of γ_s

We will study the hadronization condition as a function of γ_s which may take large values. We note that γ_s cannot rise above a limit, to be determined from a similar consideration as is the maximum (critical CR) value of

$$\gamma_q^{\mathrm{CR}} = \exp(m_\pi/2T). \tag{4}$$

At this value, the Bose distributions of pions diverges. As γ_s increases, the same will happen in the strange hadron sector, and indeed this will occur first to the lightest particle with considerable hidden strangeness content, i.e., $\eta(548)$. Naively, one could expect that $\gamma_s^{\mathrm{CR}} = \exp(m_\eta/2T)$. However, η, unlike the spin 1 $\phi(1020)$, is not a (nearly) pure $\bar{s}s$ state.

The quark structure of $\eta(548)$ and $\eta'(958)$ can be written as

$$\eta = \frac{u\bar{u} + d\bar{d}}{\sqrt{2}}\cos\phi_p - s\bar{s}\sin\phi_p, \tag{5}$$
$$\eta' = \frac{u\bar{u} + d\bar{d}}{\sqrt{2}}\sin\phi_p + s\bar{s}\sin\phi_p.$$

A study of numerous experimental results, and in particular of $Z^0 \to$ hadrons, shows that $\sin^2\phi_p = 0.45 \pm 6$, indicating that $\eta(548)$ has 45% strangeness content [9]. This arises from the SU(3)-flavor octet state content of 67% reduced by SU(3)-symmetry breaking mixing with the 33% strangeness content of the singlet $\eta'(958)$.

In order to count the yield of the η, we introduce its fugacity Υ_η. The fractional contribution to the partition function is

$$\ln Z_\eta = -\int \mathrm{d}V \frac{\mathrm{d}^3p}{(2\pi)^3} \ln\left(1 - \Upsilon_\eta \mathrm{e}^{\frac{-E_\eta}{T}}\right), \tag{6}$$

with $E_\eta = \sqrt{m_\eta^2 + p^2}$. We focus our attention on the dominant, directly produced η. The incremental per unit volume η yield is

$$\frac{\mathrm{d}N_\eta}{\mathrm{d}V} = \Upsilon_\eta \frac{\partial[\mathrm{d}\ln Z_\eta/\mathrm{d}V]}{\partial\Upsilon_\eta} = \int \frac{\mathrm{d}^3p}{(2\pi)^3} \frac{1}{\Upsilon_\eta^{-1}\mathrm{e}^{\frac{E_\eta}{T}} - 1}. \tag{7}$$

More specifically, the rapidity density is

$$n_\eta \equiv \frac{\mathrm{d}N_\eta}{\mathrm{d}y} = \frac{\mathrm{d}V}{\mathrm{d}y} \times \frac{\mathrm{d}N_\eta}{\mathrm{d}V}. \tag{8}$$

The "normalization" $\mathrm{d}V/\mathrm{d}y$ which comprises the transverse dimension at hadronization, and the longitudinal incremental volume, is arising from kinetic expansion processes driven by the initial state formation mechanisms. These have to be obtained by methods beyond the scope of this work. However, we note that in the longitudinally scaling limit for ideal fluid hydrodynamic evolution of the initial state, at all times the entropy rapidity density remains constant, $\mathrm{d}S/\mathrm{d}y = \text{Const}$. Since the particle multiplicity is defined by the value of $\mathrm{d}S/\mathrm{d}y$, the total hadron multiplicity is not affected by our ensuing study of hadronization for different chemical freeze-out temperatures. The total charge particle rapidity density is a consequence of initial processes which are beyond the physics reach of this work.

We now relate the η-fugacity Υ_η to the light and strange quark fugacities γ_q and γ_s. In the SHM, the probability of the production of η is weighted with the yield of strange and light quark pairs in proportion of their contribution to the quark content in the particle formed. Thus,

$$\Upsilon_\eta = \gamma_q^2\cos^2\phi_p + \gamma_s^2\sin^2\phi_p < \mathrm{e}^{m_\eta/T}. \tag{9}$$

The upper limit is set at the phase space divergence point. Specifically, considering $\eta(548)$ with its 45% strangeness content, we find from (9) a maximal value $\gamma_s < 10.4$ for the hadronization conditions of interest in this work, i.e., $\gamma_q \to \mathrm{e}^{m_\pi/2T}$ and $T \to 140\,\mathrm{MeV}$. Thus we set as the range of interest $0 < \gamma_s < 10$.

This upper limit is the most stringent constraint for γ_s: it is more stringent than the one which arises from the consideration of the ϕ-meson,

$$\Upsilon_\phi = \gamma_s^2 < \mathrm{e}^{m_\phi/T}, \tag{10}$$

due to the greater ϕ-mass. Similarly, the constraint on γ_s based on the kaon condensation (in the presence of negligible chemical potentials) is

$$\Upsilon_K = \gamma_s\gamma_q < \mathrm{e}^{m_K/T}. \tag{11}$$

is less severe.

To confirm the functional dependence on γ_i, (9), we show that it is consistent with the requirement that the fugacity γ_i, allows for the count of the valence quark content in hadrons. We look at γ_s, which allows for the count of all strange and antistrange quarks by the relation

$$s + \bar{s} = \gamma_s \frac{\partial \ln Z}{\partial\gamma_s}. \tag{12}$$

The contribution of η to the strangeness count thus is

$$\begin{aligned}(s+\bar{s})_\eta &= \frac{\gamma_s}{\Upsilon_\eta}\frac{\partial\Upsilon_\eta}{\partial\gamma_s}\Upsilon_\eta\frac{\partial\ln Z_\eta}{\partial\Upsilon_\eta},\\ &= 2\frac{\gamma_s^2\sin^2\phi_p}{\gamma_q^2\cos^2\phi_p + \gamma_s^2\sin^2\phi_p}N_\eta,\end{aligned} \tag{13}$$

which is the required result. A similar procedure can be followed to show that

$$(q+\bar{q})_\eta = 2\frac{\gamma_q^2\cos^2\phi_p}{\gamma_q^2\cos^2\phi_p + \gamma_s^2\sin^2\phi_p}N_\eta. \tag{14}$$

We conclude that (9) defines the η-fugacity in terms of light and strange quark fugacities.

3.3 Range of γ_s of interest

When γ_s increases, the η-fugacity increases rapidly, but, even at $\gamma_s = 5$, it is well below the Bose singularity. For $T = 160\,\mathrm{MeV}$, the singularity would be just above $\gamma_s = 8$. However, the fall-off of the expected hadronization temperature (see below) moves this towards a twice as large value. One may wonder how large a value of γ_s is physically consistent, and in particular, if an associate decrease in the value of T makes sense.

In qualitative terms, this type of parameter evolution and correlation is fully consistent with the picture of rapid transverse expansion of the QGP fireball. This expansion can lead to supercooling which pushes the hadronization temperature lower. At the same time, the preserved yield of strangeness requires that γ_s increases.

We now look at the possible range of expected values of γ_s in more detail. It can be expected that, for LHC extreme conditions, the strangeness phase space has been chemically saturated at a temperature *larger* than the strange quark mass: $T_1 > m_s$. Moreover, in the QGP phase, there is a residual strange quark mass $m_s > T$, where T is the final hadronization temperature. While the precise value of m_s depends on the momentum scale at which it is measured, we will assume in this semi-quantitative discussion that $m_s(1\,\mathrm{GeV}) \simeq 180\,\mathrm{MeV}$. Conservation of the strangeness rapidity yield in the expansion from T_1 to T implies, by comparison of the relativistic phase space size,

$$(\mathrm{d}V_1 T_1^3) W(m_s/T_1) = \gamma_s^{\mathrm{Q}} \times (\mathrm{d}V T^3) W(m_s/T), \qquad (15)$$

where γ_s^{Q} is the quark-side hadronization phase space occupancy; for the definition of $W(x)$, see (18). For $0 < x < 1$, $W(x)$ is slowly changing and close to its asymptotic value $W(x = 0) = 2$. Entropy conservation further requires that $\mathrm{d}V_1 T_1^3 = \mathrm{d}V T^3 = \mathrm{Const}$.

For $T_1 \simeq 1.5T$, and noting that $T_1 > m_s > T$, we obtain, as a solution of (15), $\gamma_s^{\mathrm{Q}} \simeq 1.5$. In the hadronization process, this value increases by a significant factor which we can obtain comparing the phase space of strange hadrons in QGP with that hadron phases (we omit as is customary the upper index H, i.e., $\gamma_s^{\mathrm{H}} \to \gamma_s$):

$$\begin{aligned} &\gamma_s^{\mathrm{Q}} \times W(m_s/T) \qquad (16)\\ &= \gamma_s \times \sum_i \tilde{W}(m_i/T) \\ &\quad + \gamma_s^2 \times \sum_j \tilde{W}(m_j/T) + \gamma_s^3 \times \sum_k \tilde{W}(m_k/T). \end{aligned}$$

The sums run over single, double and triple strange (s and $\bar{s}$) hadrons, respectively. $\tilde{W}$ differs from W in that it comprises appropriate hadron fugacities for each particle; the appropriate expressions are seen in more detail in (17).

The strangeness QGP-to-HG aspect ratio, i.e., the ratio of the phase space size seen in (16) up to the coefficients γ_s^{Q}, γ_s shows that it grows with decreasing temperature; see Fig. 19.3 in [3]. This is further strongly amplifying by a factor as large as four the final observed γ_s. A QGP phase value $\gamma_s^{\mathrm{Q}} \simeq 1.5$ may become $\gamma_s \simeq$ 5–10 on the hadron side. As we shall see, the decrease of T with increasing γ_s compensates, in part, the increase with γ_s in the yields of strange hadrons. We will thus consider the range $0.5 < \gamma_s < 10$, as that is where most of the variation in the considered observables is seen and the actual physical conditions are expected to occur. The lower limit underscores the comparison with the equilibrium model $\gamma_s = \gamma_q = 1$ behavior. The upper limit $\gamma_s < 10$ is within the range of allowed values of γ_s we have obtained in Sect. 3.2.

4 Predictions

4.1 SHM parameter values at LHC top energy

With the assumptions outlined in Sect. 3.1, we solve for the best set of SHM model parameters. A precise solution is always found in the considered range of γ_s, and also for the increased value of E/TS for the case of chemical equilibrium. This of course does not guarantee that, e.g., our baryochemical potential is correctly chosen. The results we show are not entirely smooth as we allow for a small error in the constraints and conditions, and thus the solution for the parameters is not a precise algebraic result, but a most likely value of a quasi-fit, which has a $\chi^2 \simeq 0$.

The resulting statistical parameters T, γ_q^{CR}, μ_{B}, and μ_S are shown, in Fig. 1, as a function of $0.5 \le \gamma_s \le 10$. Note that through our study of chemical non-equilibrium, $\gamma_q \simeq \gamma_q^{\mathrm{CR}}$. We see that an increasing value of γ_s is accompanied by a considerable reduction of the hadronization temperature, which drops from the value $T = 140\,\mathrm{MeV}$, near $\gamma_s = 2.4$ and $\gamma_q = 1.6$, down to $T = 110\,\mathrm{MeV}$. At the favorite value $\gamma_s = 5$, the expected LHC hadronization temperature is $T = 125\,\mathrm{MeV}$ for the chemical non-equilibrium. The chemical equilibrium result at $T = 156$ implies a chemical potential $\mu_{\mathrm{B}} = 2.6\,\mathrm{MeV}$, and this value is also found for the chemical non-equilibrium model for $\gamma_s = 5$. We explain why μ_{B} remains unchanged at the end of Sect. 5. For μ_S, we see a slight reduction by 10% from equilibrium model value at $0.52\,\mathrm{MeV}$ as is appropriate considering the results presented in Fig. 5. Our estimate of the chemical parameters at LHC are considerably different from those proposed by others as in [10], where $\mu_{\mathrm{B}} = 1\,\mathrm{MeV}$ and $\mu_S = 0.3\,\mathrm{MeV}$ is proposed. We note that our baryochemical potential is considerably greater. We will discuss the experimental consequences at greater length in Sect. 5.

It is of considerable interest to study the physical properties at hadronization: the pressure P, the energy density $\epsilon = E/V$, the entropy density $\sigma = S/V$, and the net baryon density $\nu = B/V$. In general, the non-equilibrium hadronization occurs from a state of higher density, as is seen in Fig. 2, comparing the lines with the SHM equilibrium cross. This is, in particular, true for the entropy density. With increasing γ_s, all density decreases, and the drop in temperature is a more important influence than the large increase in relative strangeness yield. Despite a significant increase in μ_{B} with increasing γ_s, the net baryon density decreases modestly. It is very small, bordering on the value $\nu = 0.001\,\mathrm{fm}^{-3}$.

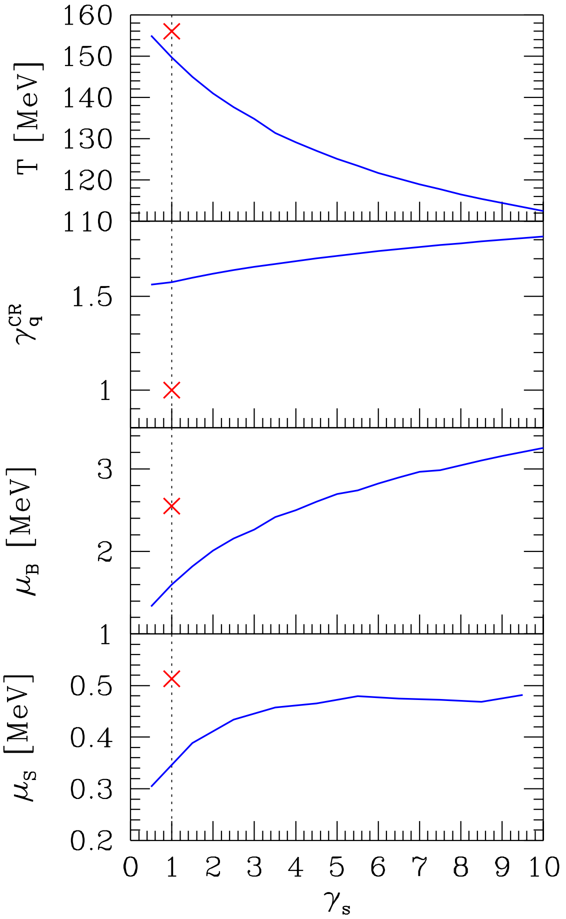

Fig. 1. (Color online) The values of T, $\gamma_q^{\rm CR}$, $\mu_{\rm B}$, and μ_S as a function of varying γ_s, consistent with the hadronization model assumptions outlined in Sect. 3.1. The equilibrium model results are crosses at $\gamma_s = 1$ for $\gamma_q = 1$

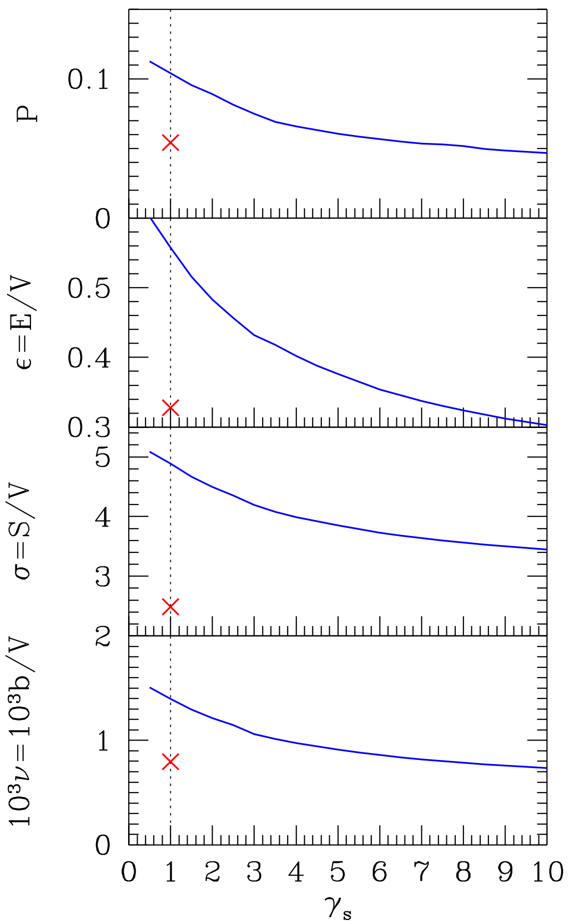

Fig. 2. (Color online) Pressure P [GeV/fm^3], energy density ϵ [GeV/fm^3], entropy density $\sigma = S/V$ [1/fm^3], net baryon density $\nu = (B - \overline{B})/V = b/V$ [1/fm^3], for non-equilibrium SHM. Cross at γ_s for chemical equilibrium

4.2 Particle yield ratios and determination of γ_s

There is approximate charge symmetry with positives h^+ and negatives h^- having a very similar yield. The difference will be discussed further below. The total charged hadron yield will be denoted

$$h = h^+ + h^- \equiv p + \bar{p} + \pi^+ + \pi^- + K^+ + K^-$$

and is evaluated after weak decay of hyperons and $K_{\rm S,L}$. Similarly the total yield of neutrals:

$$h^0 \equiv \pi^0 + n + \bar{n}.$$

The top panel, in Fig. 3, shows the $2h^0/h$ ratio, which varies by ±10% in the range of γ_s considered, with the charge symmetric value $2h^0/h = 1$ arising at $\gamma_s = 3.3$.

In the lower three panels, we focus our interest on ratios of some interest for the determination of γ_s. We present the ratio η/π^0 which rises by nearly 50% compared to the equilibrium model expectation, see the crosses at $\gamma_s = 1$, computed for $\gamma_q = 1$ and $T = 156$ MeV. This ratio is observed by reconstruction of the invariant di-photon mass. This observable shows a relatively small variation with γ_s, which can be understood as a result of competition between γ_s and γ_q, see (9), which is accompanied by the decrease of T with increasing γ_s. We record that the expectation for the non-equilibrium hadronization at LHC is

$$0.07 < \frac{\eta}{\pi^0} < 0.12.$$

This interesting observable may also not have the sensitivity required to distinguish the models, or help determine γ_s.

In the panel below, we show the $(K^+ + K^-)/h$ ratio. This ratio is rising, for large γ_s, to a value near 0.23 almost double the "standard" chemical equilibrium value at 0.12. However, for $\gamma_s = 5$, we see a more modest increase by 50%. We record for LHC that

$$0.12 < \frac{K^+ + K^-}{h^+ + h^-} < 0.23.$$

More spectacular is the expected increases in the $2\phi/h$ ratio. The chemical equilibrium value of 0.015 is seen to rise 4-fold, and at $\gamma_s = 5$, we still see a very noticeable increase by a factor 2.5. This is a very important observable of the condition of hadronization. We record our LHC expectation:

$$0.015 < \frac{2\phi}{h^+ + h^-} < 0.06.$$

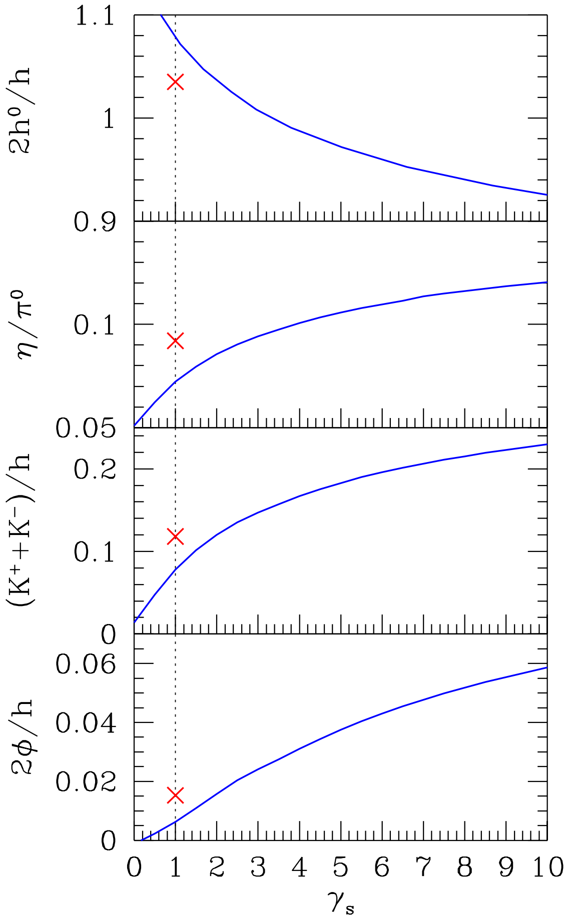

Fig. 3. (Color online) The predicted yield ratios as function of γ_s, from top to bottom: ratio of neutral to charged hadrons $2h^0/h$, η/π^0, $(K^+ + K^-)/h$ and $2\phi/h$ as a function of γ_s. The cross indicates the chemical equilibrium model prediction. All yields after weak decay of hyperons and $K_{\rm S,L}$

The behavior of the baryon yields is shown in Fig. 4 where the total, nearly matter–antimatter symmetric yields of protons, and the three hyperon families are shown, normalized by the total charged hadron yield h. The lines, from top to bottom, are for $(p+\bar{p})/h$, $(\Lambda+\overline{\Lambda})/h$, $(\Xi^- + \overline{\Xi}^+)/h$ and $(\Omega^- + \overline{\Omega}^+)/h$. We note that for a large γ_s, a considerable change in the expected baryon populations ensues, with proton yield decreasing (due to decrease in T associated with the increase in γ_s) while the more strange the hyperon is, the more it is enhanced compared to chemical equilibrium expectations. Interestingly, these relative yields saturate with increasing γ_s, as the effect of temperature decrease competes with the increase due to rising γ_s. Note that we have shown, in Fig. 4, the total hadron yields after all weak decays have occurred. We summarize our LHC expectations:

$$0.07 > \frac{p+\bar{p}}{h^+ + h^-} > 0.04,$$

$$0.02 < \frac{\Lambda+\overline{\Lambda}}{h^+ + h^-} < 0.04,$$

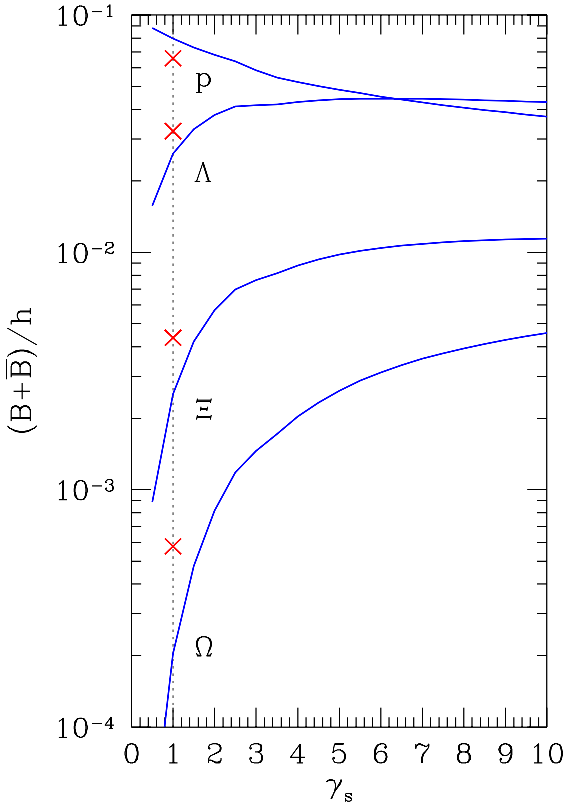

Fig. 4. (Color online) (Strange) baryon ratios with charge hadron multiplicity $(p+\bar{p})/h$, $(\Lambda+\overline{\Lambda})/h$, $(\Xi^- + \overline{\Xi}^+)/h$ and $(\Omega^- + \overline{\Omega}^+)/h$, after all weak decays occurred. Crosses denote the chemical equilibrium result

$$0.004 < \frac{\Xi^- + \overline{\Xi}^+}{h^+ + h^-} < 0.015,$$

$$0.0006 < \frac{\Omega^- + \overline{\Omega}^+}{h^+ + h^-} < 0.004.$$

5 Measurement of the baryochemical potential

5.1 Strangeness conservation

An interesting challenge, at LHC, will be the measurement of chemical potentials. We recall that μ_S is directly related to $\mu_{\rm B}$ should hadron emission at each rapidity occur such that there is local strangeness balance, i.e., "conservation". This relates the two chemical potentials as we shall next discuss. Otherwise, if emission of hadrons were to reflect on the QGP conditions, we would expect $\mu_S = 0$ and this would generate a buildup of residual strangeness in a distillation process [11]. We tacitly assumed, and continue in this way now, that at LHC, in each rapidity region, local conservation of strangeness prevails. We present a set of results which will allow one, given appropriate experimental sensitivity, to determine the value of μ_S.

Strangeness conservation establishes a relation between the chemical potentials [12]. While this relationship is simplified for the case $\mu_i/T \ll 1$, the presence of $\gamma_s \gg 1$

introduces new elements and we reinspect the relationship. Using, at first, the quark fugacity notation for convenience, the open strangeness sector partition function is, in the Boltzmann approximation here appropriate,

$$\ln Z_s \equiv \gamma_s\gamma_q F_K\left(\frac{\lambda_s}{\lambda_q}+\frac{\lambda_q}{\lambda_s}\right)+\gamma_s\gamma_q^2 F_{\mathrm{Y}}\left(\lambda_s\lambda_q^2+\frac{1}{\lambda_s\lambda_q^2}\right)$$
$$+\gamma_s^2\gamma_q F_{\Xi}\left(\lambda_s^2\lambda_q+\frac{1}{\lambda_s^2\lambda_q}\right)+\gamma_s^3 F_{\Omega}\left(\lambda_s^3+\frac{1}{\lambda_s^3}\right). \tag{17}$$

The phase space factors,

$$F_i(T)=\frac{VT^3}{2\pi^2}\sum_{k\in i} g_k W(m_k/T),\quad W(x)=x^2K_2(x), \tag{18}$$

comprise all contributing hadron states “k” with quantum number “i”. $W(x)=x^2K_2(x)\overset{x\to 0}{\to} 2$ is the relativistic phase space integral in the classical limit, which for large x behaves as $W(x)\propto x^{3/2}\exp(x/T)$. A series of these terms represents quantum statistics; see (19).

The strangeness conservation condition,

$$\langle s\rangle-\langle\bar{s}\rangle=\frac{\lambda_s\partial\ln Z}{\partial\lambda_s}=0,$$

yields for small values of chemical potentials, in units of T,

$$\mu_{\mathrm{B}}-\mu_S+2(\mu_{\mathrm{B}}-2\mu_S)\frac{\gamma_s}{\gamma_q}\frac{F_{\Xi}}{F_{\mathrm{Y}}}+3(\mu_{\mathrm{B}}-3\mu_S)\frac{\gamma_s^2}{\gamma_q^2}\frac{F_{\Omega}}{F_{\mathrm{Y}}} \tag{19}$$
$$=\mu_S\left(\frac{F_K}{\gamma_q F_{\mathrm{Y}}}+\frac{\gamma_s\tilde{F}_K(2m_K)}{4F_{\mathrm{Y}}}+\frac{\gamma_q\gamma_s^2\tilde{F}_K(3m_K)}{9F_{\mathrm{Y}}}+\dots\right).$$

The right hand side presents the three first terms of the kaon Bose integral expansion which keeps terms of the same order as those belonging to Ξ and Ω in the balance. These are not entirely negligible for large γ_s. We solve (19) and show, in Fig. 5, μ_{B}/μ_S as a function of T:

$$\frac{\mu_{\mathrm{B}}}{\mu_S}=f(T;\gamma_q,\gamma_s). \tag{20}$$

The dashed curve is the equilibrium case for $\gamma_s=\gamma_q=1$, where we marked the RHIC hadronization condition $\mu_{\mathrm{B}}/\mu_S=5$ with a cross. The closest solid line to this result is for $\gamma_q=\mathrm{e}^{m_{\pi^0}/T}$ and $\gamma_s\to 0$. The following solid lines are, in sequence from upper right, for $\gamma_s=0.5,\ 1,\ 3,\ 5,\ 7,\ 10$. The cross near the $\gamma_s=3$ line, at $\mu_{\mathrm{B}}/\mu_S=4.6$, corresponds to the RHIC chemical non-equilibrium hadronization condition.

These results allow, aside of gauging the LHC values of chemical potentials, also for an easy comparison with and cross check of other work addressing LHC and RHIC environments with conserved strangeness. We recall that many particle ratios are directly determined by chemical potentials, e.g., $K^+/K^-=\exp(2\mu_S/T)$ and $\overline{\Xi}^+/\Xi^-=\exp((2\mu_{\mathrm{B}}-4\mu_S)/T)$. This obviously leads to consistency conditions in the particle–antiparticle asymmetry sensitive particle ratios.

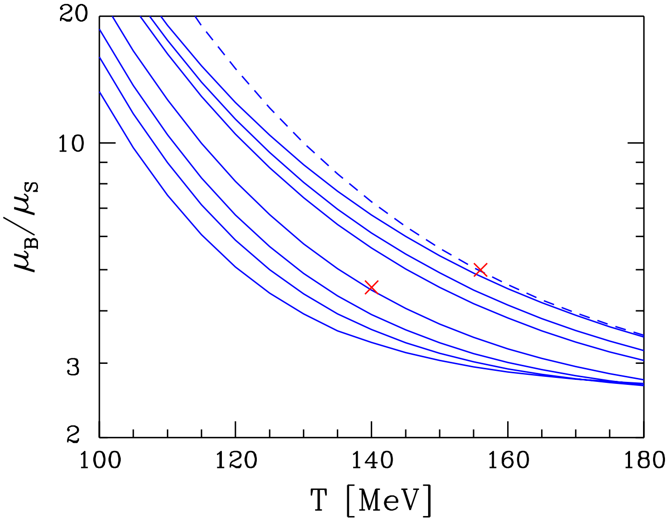

Fig. 5. (Color online) μ_{B}/μ_S as a function of T: From top right to left $\gamma_s=0,\ 0.5,\ 1,\ 3,\ 5,\ 7,\ 10$, at $\gamma_q=\exp(m_{\pi^0}/T)$. The dashed (red) line shows the chemical equilibrium model result at $\gamma_s=1$ and $\gamma_q=1$. Crosses correspond to RHIC freeze-out conditions both in equilibrium (at dashed line) and non-equilibrium

5.2 Hadron–antihadron asymmetry

In order to measure chemical potentials, we need to be able to measure the particle–antiparticle asymmetry. This is not an easy task at LHC as we shall see. Up to RHIC energy, it was customary to study the ratio of antiparticle yields to particle yields, such as $\overline{\Lambda}/\Lambda$. At LHC, the strategy has to slightly change. We consider normalized particle–antiparticle difference yields,

$$\Delta N_i=\frac{\bar{n}_i-n_i}{\bar{n}_i+n_i}, \tag{21}$$

where n_i is the rapidity density $\mathrm{d}N/\mathrm{d}y$ of the charged particles $i=K^+,\ p,\ \Lambda,\ \Xi,\ \Omega$ and antiparticles. We omitted intentionally the pion from this list, as it is the dominant component of the unidentified particle hadron asymmetry; we will address this next. Below, we will omit the factor $\mathrm{d}/\mathrm{d}y$ as the expressions we state are valid more generally.

The most accessible observable,

$$\Delta h\equiv\frac{h^+-h^-}{h^++h^-}, \tag{22}$$

composed of unidentified charged hadrons, is very hard to measure precisely, for
(i) there are distortions possible by partial acceptance of weak decays, and
(ii) this variable assumes a comparatively small value at LHC. Moreover, this is also an observable hardest to interpret in a simple and transparent theoretical model. We find that its magnitude for LHC will be

$$\Delta h=(0.5\text{–}0.6)10^{-3},$$

for all values of $\gamma_s\geq 1$, as is shown in Fig. 6. The differ-

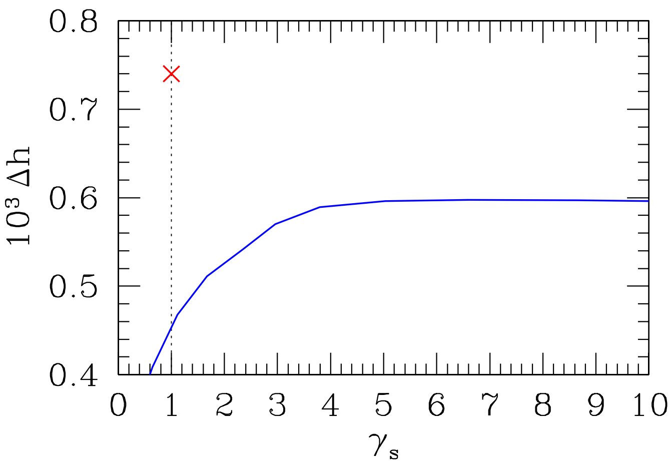

Fig. 6. Δh as a function of γ_s. A cross indicates an equilibrium model result

ence in Δh between the equilibrium and non-equilibrium result is due to the increased entropy and thus the hadron multiplicity content of the chemical non-equilibrium case. The variable Δh has been recognized already in the study of SPS reactions as a sensitive probe of entropy production [12,13].

Should a way to measure Δh of this magnitude with reasonable precision be found at LHC, this would provide a model independent measure of the value of the baryochemical potential $\mu_{\rm B}$. To see this, we solve (fit) the SHM with a fixed assumed value of Δh. In the chemical equilibrium version of SHM, we find, at $\gamma_s = \gamma_q = 1$, in the T–$\mu_{\rm B}$ plane the constraint lines determined by the assumed values of Δh, shown in the top panel of Fig. 7. From left to right, we have considered three benchmark values, $\Delta h = 0.001$ (top LHC energy), $\Delta h = 0.01$ (top RHIC energy), and $\Delta h = 0.1$ (top SPS energy, central rapidity region). At SPS, top energy in the S–Pb interactions, we have studied this variable (called $D_Q \simeq 0.009$) in the context of the exploration of the specific entropy per baryon [12,13], and the results we present here are in agreement with this early study of SPS hadron multiplicities.

For non-equilibrium case, with $\gamma_q = \gamma_q^{\rm CR}$, the corresponding result is shown in the second top panel. The nearly vertical lines are solutions of the following conditions imposed: strangeness conservation, charge-to-baryon ratio and Δh, as a function of $\mu_{\rm B}$. For each value of T, there is a specific value of γ_s indicated in the next lower panel, and again, we see nearly a vertical line. Both these results imply that while the value of T and γ_s are not much constrained by the measurement of just one single observable Δh, the value of $\mu_{\rm B}$ is already highly constrained.

Why this is the case is understood inspecting the bottom panel in Fig. 7. We show the resulting value of thermal energy per baryon E/b. These turn out to be highly localized regions. Thus, Δh is for a wide range of other statistical parameters closely related to the value of energy per baryon, or equivalently, entropy per baryon. The connecting dashed line in the bottom panel guides the eye. A check of E/TS also confirms that these solutions produce the expected result which is otherwise introduced as a constraint.

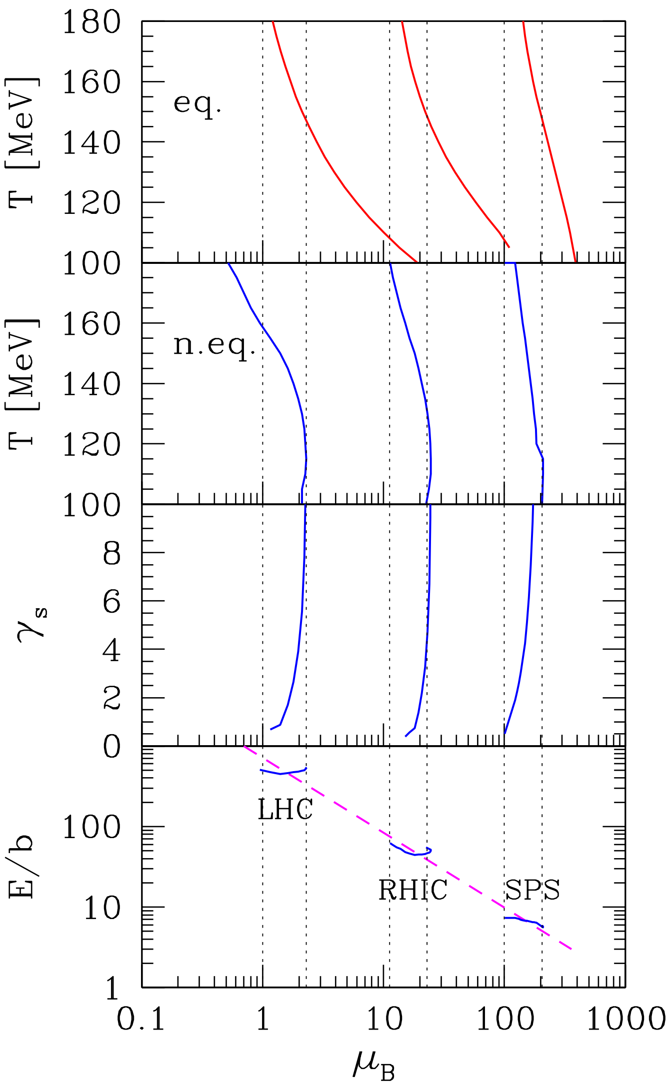

Fig. 7. (Color online) Δh constraint from left to right for LHC $\Delta h = 0.001$; for RHIC $= 0.01$ and for SPS top energy $= 0.1$. Top panel: chemical equilibrium SHM, T–$\mu_{\rm B}$ plane, bottom three panels: chemical non-equilibrium, from top to bottom T, followed by γ_s and $\mathrm{d}E/\mathrm{d}b$ combined with $\mu_{\rm B}$. In the bottom panel the dashed line indicate the systematics of the behavior regarding the value of thermal energy per baryon. Vertical dotted lines brace the extreme allowable values of $\mu_{\rm B}$

Thus, we learn that just the single "measured" value Δh is enough to constrain a rather narrow range of $\mu_{\rm B}$. This result is indicated by the vertical dotted line, which we place bracing the domains of $\mu_{\rm B}$ that are allowed. Inspecting the equilibrium model intercept, we realize that this singles out a domain of T which is a result of data fits with this constraint. This explains why $\mu_{\rm B}$ is usually determined in a model independent way within the SHM, with little if any difference present between the different model variants, provided that the experimental data used in the fit comprises explicitly, or implicitly, Δh. For example, the study of the impact parameter dependence at RHIC using different SHM model variants produced $\mu_{\rm B}$

and μ_S which cannot be distinguished (see bottom panel of Fig. 1 in [14]).

5.3 Identified particle–antiparticle asymmetries

For the identified particles, the normalized particle–antiparticle differences can be closely and analytically related to the value of the chemical potential. For example, the kaon asymmetry is directly related to the strangeness chemical potential μ_S:

$$\Delta K \equiv \frac{K^+ - K^-}{K^+ + K^-} \simeq \tanh\frac{\mu_S}{T} \to \frac{\mu_S}{T}. \tag{23}$$

We have, for simplicity, not considered the ϕ-meson decay contributions which increase the normalizing yield but do not alter the difference.

We show the actual, with all decays, ΔK as a thick solid line in the top panel of Fig. 8 (bottom line in this top panel). The very top short-dashed line in the panel (red on-line) is the ratio μ_S/T. The thick long-dashed line excludes from the ratio the contamination by the decay $\phi \to K^+ + K^-$. The fully weak decay contamination corrected results are the thin (solid respectively dashed) lines at the top of the parallel lines, and are shown for both the full result (solid lines) and the ϕ-decay corrected result (long dashed). The parallel line regions are where the acceptance of weak decays is partial and/or the correction is incomplete. After the removal of the ϕ-decay dilution of the kaon yields, (23) should read

$$\Delta K \simeq 0.9\frac{\mu_S}{T}. \tag{24}$$

The slight reduction from the analytical formula (23) is due to the strong decay contributions of hyperon resonances decaying emitting a kaon. Because of the smallness of ΔK, the baryon asymmetry in the hyperon resonances leaves this small but visible imprint of this result.

The chemical equilibrium result (cross before and circle after weak decays) is also indicated in Fig. 8. These are, in general, larger than the analytical results (short-dashed lines) except in the case of $\Delta\ K$.

For baryons there are four particle–antiparticle differentials, which are shown below ΔK, in Fig. 8. We expect for protons

$$\Delta p \equiv \frac{p - \bar{p}}{p + \bar{p}} = \tanh\frac{\mu_{\mathrm{B}}}{T} \to \frac{\mu_{\mathrm{B}}}{T}. \tag{25}$$

The thin solid line in the second panel from the top which corresponds to removed weak decays compares well to the analytical results; see the short-dashed line. The thick solid line at the bottom of the parallel lines includes in Δp the contamination from weak decays of Λ and $\overline{\Lambda}$, and the region in between spans all possible WD contamination.

Once the weak decay contributions $\Omega, \Xi \to \Lambda$ and $\overline{\Omega}, \overline{\Xi} \to \overline{\Lambda}$ are removed, we have further

$$\Delta\Lambda \equiv \frac{\Lambda - \overline{\Lambda}}{\Lambda + \overline{\Lambda}} = \tanh\frac{\mu_{\mathrm{B}} - \mu_S}{T} \to \frac{\mu_{\mathrm{B}} - \mu_S}{T}. \tag{26}$$

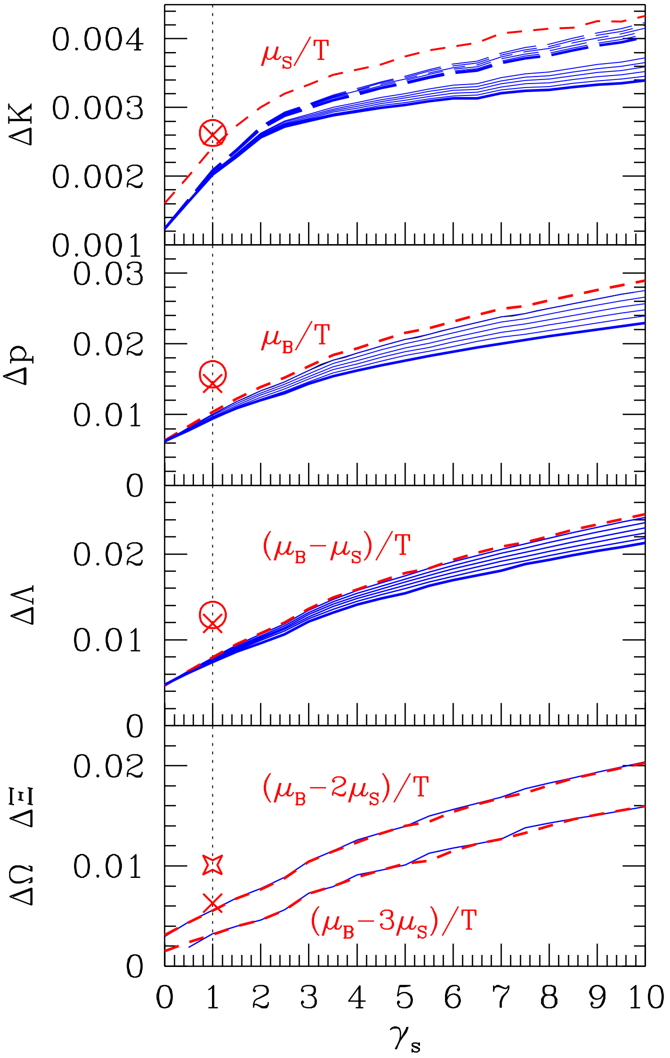

Fig. 8. (Color online) Solid lines: the relative particle–antiparticle asymmetry as a function of γ_s, from top to bottom ΔK, Δp, $\Delta\Lambda$ and together in bottom panel $\Delta\Xi$ and $\Delta\Omega$. The short-dashed line (red) is the analytical result, given in terms of μ_i/T (see text). The range of weak decay corrections is shown by parallel lines with the most decay contaminated result being the bottom, thick line. For ΔK we also show by a long dashed lines the result after the ϕ-decay contribution to ΔK has been removed. The equilibrium model results are shown as crosses (after weak decays) and circles (corrected for weak decays) at the $\gamma_s = 1$ vertical dotted line. The diamond symbol in the bottom panel is the chemical equilibrium result for $\Delta\Xi$, different from the cross for $\Delta\ \Omega$

The thin line, in the $\Delta\Lambda$ panel, is nearly indistinguishable from this result. The thick solid line includes all weak decays.

There is no significant contamination of Ξ^- and $\overline{\Xi}^+$ and thus we have

$$\Delta\Xi \equiv \frac{\Xi^- - \overline{\Xi}^+}{\Xi^- + \overline{\Xi}^+} = \tanh\frac{\mu_{\mathrm{B}} - 2\mu_S}{T} \to \frac{\mu_{\mathrm{B}} - 2\mu_S}{T}, \tag{27}$$

and similarly for the Ω^-

$$\Delta\Omega \equiv \frac{\Omega^- - \overline{\Omega}^+}{\Omega^- + \overline{\Omega}^+} = \tanh\frac{\mu_\mathrm{B} - 3\mu_S}{T} \to \frac{\mu_\mathrm{B} - 3\mu_S}{T}, \quad (28)$$

both shown in the bottom panel of Fig. 8.

The values of the five observables $\Delta N_i, i = p, K, \Lambda, \Xi, \Omega$ are determined by three parameters, two chemical potentials μ_B, μ_S and the temperature T. The other relevant parameter value is $\lambda_{I3} \to 1$ considering the isospin bath of numerous pions, yielding $T \ln \lambda_{I3} \ll \mu_\mathrm{S}$ to a great precision. The expected asymmetry ΔN_i is at %-level and the weak decay of hyperons allow unique identification of these particles. It is quite possible that the measurement of these variables will succeed.

When measured, the 5 different ΔN_i which depend on two parameters μ_B/T and μ_S/T would check for consistency with the SHM model. This consistency is further tightened due to the strangeness conservation relation of $\mu_\mathrm{B}/\mu_S = 4$–5; see Sect. 5.1. The strangeness conservation constraint and through it the SHM model can be tested by transforming (23), (25), (26), (27) and (28), so we can make use of (19) and the values (20):

$$\frac{\Delta p}{\Delta K} = \frac{\mu_\mathrm{B}}{\mu_S} \simeq 4.5, \quad (29)$$

$$\frac{\Delta\Lambda}{\Delta K} = \left(\frac{\mu_\mathrm{B}}{\mu_S} - 1\right) \simeq 3.5, \quad (30)$$

$$\frac{\Delta\Xi}{\Delta K} = \left(\frac{\mu_\mathrm{B}}{\mu_S} - 2\right) \simeq 2.5, \quad (31)$$

$$\frac{\Delta\Omega}{\Delta K} = \left(\frac{\mu_\mathrm{B}}{\mu_S} - 3\right) \simeq 1.5. \quad (32)$$

These relations test the SHM and strangeness conservation; they do not differentiate model variants such as chemical equilibrium and chemical non-equilibrium.

6 Final remarks

The total multiplicity yield, as well as the yield of charmed particles, is originating predominantly in the early stage, primary parton reactions. For this reason, we did not address absolute yields of hadrons, and, similarly, we cannot study the total charm yield in the context considered here. However, one may wonder if the appearance of small but distinguished charmed meson and baryon yield does not offer an interesting and independent probe of the properties of the hadronization state, or even if it could influence the results presented.

An earlier study of charmed hadron production, in chemical equilibrium at $T = 170\,\mathrm{MeV}$, has yielded interesting insights into the relative production strengths of charmed mesons and baryons emerging at this particular hadronization temperature [10]. We will not enter into further discussion of this subject, but note that
(a) for $\gamma_s > 2$, these results imply that $D_s(c\bar{s})^+$ and its antiparticle should be the dominant charmed hadron fraction;
(b) the differences in yields between particles and antiparticles, shown in Table 3 of [10], indicate that the charm particle contributions to the asymmetries we studied are totally negligible. It appears that a measurement of the relative yield of charmed mesons and baryons will reveal the charm hadronization condition, and we hope to return to this subject soon.

The small relative number of charmed quarks and their even smaller particle–antiparticle asymmetry assures that these particles do not impact any of the results we obtained. On the other hand, these particles offer another opportunity to explore the hadronization conditions. The formation of charmed hadrons is expected to occur prior to general hadronization, considering the greater binding of charmed particles [15].

To summarize, we have presented a detailed study of the soft hadron production pattern at LHC. We discussed, in turn, relative yields such as ϕ/h and K/h which allow for insights into the hadronization conditions and help address questions related of chemical equilibrium and non-equilibrium, as well as temperature of hadron freeze-out.

Perhaps the most interesting result to pursue experimentally is the large value of γ_s expected in the hadronization of an over-saturated QGP phase. The ratios, shown in Figs. 3 and 4, are not very sensitive to the choices we made that determine the chemical potentials μ_B and μ_S; they probe primarily the interplay between the γ_s and T. We note further that most these ratios, at the favored value $\gamma_s \simeq 5$, differ considerably from the chemical equilibrium model expectations. The relatively large value of γ_s we expect at LHC, twice as large as our analysis finds at RHIC, derives from a larger absolute density of strangeness at hadronization of the deconfined phase, combined with a lower prevailing temperature as expected in deeper expansion supercooling. Indeed, while at RHIC $\gamma_s^\mathrm{QGP}|_\mathrm{hadronization} \leq 1$, at LHC we expect $\gamma_s^\mathrm{QGP}|_\mathrm{hadronization} \to 1.5$–2. The difference in the phase space size of QGP with HG then leads to $\gamma_s \simeq\ 5$.

We have further presented an in depth discussion of particle–antiparticle asymmetries which address the challenge of chemical and strange quark chemical potential measurement. Since the particle–antiparticle yield difference is small compared to each individual yield, a special effort will need to be made to acquire these difference ratios $\Delta N_i \simeq 0.1$–4% at the level of 10% or better.

Acknowledgements. Work supported by a grant from the U.S. Department of Energy DE-FG02-04ER41318. LPTHE, Univ. Paris 6 et 7 is Unité mixte de Recherche du CNRS, UMR7589.

References

1. H.Z. Huang, J. Rafelski, AIP Conf. Proc. **756**, 210 (2005) [hep-ph/0501187]
2. M.J. Fromerth, J. Rafelski, Hadronization of the quark universe, astro-ph/0211346

3. J. Letessier, J. Rafelski, Hadrons and quark-gluon plasma, Cambridge Monogr. Part. Phys. Nucl. Phys. Cosmol. **18**, 1 (2002)
4. J. Letessier, J. Rafelski, Hadron production and phase changes in relativistic heavy ion collisions, nucl-th/0504028
5. P. Braun-Munzinger, K. Redlich, J. Stachel, Particle production in heavy ion collisions, nucl-th/0304013, and references therein
6. G. Torrieri, W. Broniowski, W. Florkowski, J. Letessier, J. Rafelski, SHARE: Statistical hadronization with resonances, nucl-th/0404083; Comp. Phys. Com. **167**, 229 (2005), see www.physics.arizona.edu/˜torrieri/SHARE/share.html
7. S. Wheaton, J. Cleymans, THERMUS: A thermal model package for ROOT, hep-ph/0407174; J. Phys. G **31**, S1069 (2005).
8. P. Petreczky, F. Karsch, E. Laermann, S. Stickan, I. Wetzorke, Nucl. Phys. Proc. Suppl. **106**, 513 (2002); F. Karsch, E. Laermann, Thermodynamics and in-medium hadron properties from lattice QCD, hep-lat/0305025, in: Quark gluon plasma III, edited by R.C. Hwa, et al., pp. 1–59 (Singapore, 2004)
9. V. Uvarov, Phys. Lett. B **511**, 136 (2001) [hep-ph/0105185]
10. A. Andronic, P. Braun-Munzinger, K. Redlich, J. Stachel, Phys. Lett. B **571**, 36 (2003) [nucl-th/0303036]
11. C. Greiner, P. Koch, H. Stocker, Phys. Rev. Lett. **58**, 1825 (1987); J. Rafelski, Phys. Lett. B **190**, 167 (1987)
12. J. Letessier, A. Tounsi, U.W. Heinz, J. Sollfrank, J. Rafelski, Phys. Rev. D **51**, 3408 (1995) [hep-ph/9212210]
13. J. Letessier, A. Tounsi, U.W. Heinz, J. Sollfrank, J. Rafelski, Phys. Rev. Lett. **70**, 3530 (1993)
14. J. Rafelski, J. Letessier, G. Torrieri, Phys. Rev. C **72**, 024905 (2005) [nucl-th/0412072]
15. R.L. Thews, J. Phys. G **31**, S641 (2005) [hep-ph/0412323]